Extensive Energy Landscape Sampling of Nanotube End-Caps Reveals No Chiral-Angle Bias for Their Nucleation

Evgeni S. Penev, Vasilii I. Artyukhov, and Boris I. Yakobson*

Department of Materials Science and NanoEngineering, and Department of Chemistry, Rice University, Houston, Texas 77005, United States

ABSTRACT In the formation of a carbon nanotube (CNT) nucleus, a hemispherical fullerene end-cap, a specific pattern of six pentagons encodes what unique (*n*,*m*) chirality a nascent CNT would inherit, with many possible pentagon patterns corresponding to a single chirality. This configurational variety and its potential role in the initial stages of CNT catalytic growth remain essentially unexplored. Here we present large-scale calculations designed to evaluate the intrinsic energies of all possible CNT caps for selected chiralities corresponding to tube diameters $d \lesssim 1$ nm. Our quantitative analysis reveals that for all chiral angles χ the energy scale variability associated with the CNT caps is small, compared to that of the CNT/catalyst interface. Such a flat energy landscape cannot therefore be a dominant factor for chiral distribution and lends further credibility to interface-controlled scenarios for selective growth of single-walled CNT of desired chirality.

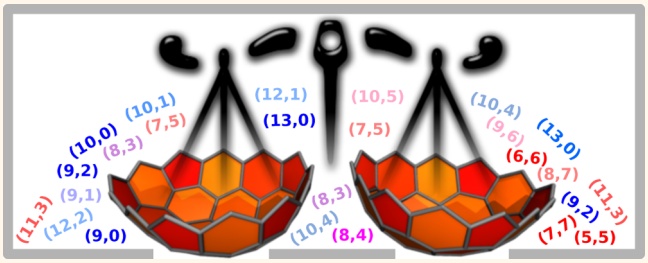

KEYWORDS: carbon nanotubes · nucleation · chiral-angle selectivity · atomistic modeling

Carbon nanotubes (CNTs) have revitalized fundamental and applied nanosciences in an unprecedented fashion. Even two decades after the seminal works[1] in the field, deep understanding of their growth mechanism is still elusive.[2] Depending on their type (*n*,*m*), nanotubes can have semiconducting or metallic electronic properties, and selectively growing nanotubes of the desired types is therefore a crucial scientific goal. Alternative to the chiral indices *n* and *m*, the nanotube type can be described by the combination of nanotube diameter $d = a/\pi(n^2 + m^2 + nm)^{1/2}$, *a* being the lattice constant, and chiral angle $\chi = \arctan(\sqrt{3}m/(m + 2n))$, which determines the direction of rolling-up of the graphene lattice,[3] to form the nanotube. Since it is usually easier to control the diameter during growth (*e.g.*, by adjusting the catalyst nanoparticle size) or to purify nanotubes by diameter after synthesis, the problem of selective CNT growth is often phrased in terms of the subgoal of controlling the chiral angle χ. Further, because it is hard to change nanotube type after growth has reached the repetitive stage, a natural focus is the nucleation stage: this is where both the diameter and chiral angle are believed to be set in.

In the pursuit of routes toward chiral selectivity,[4] the importance of the nucleation stage in the CNT growth has long been recognized and extensively studied both experimentally and theoretically for various growth scenarios.[5−15] Within the classical nucleation theory, the change in the Gibbs free energy upon formation of a sp^2 nucleus of *N* atoms is composed of a "bulk" term $\sim N$ and an edge term[7] $\sim N^{1/2}$. This energy decomposition has been well explored for the archetypal system of a graphene island on a metal substrate[16−19] as well as in the case of phase separation in graphene functionalization.[20,21] On a finite-size particle, *e.g.*, of radius *R*, the carbon nucleus has to accommodate mean curvature $\sim 1/R$ by incorporating pentagonal "defects", which leads to an elastic energy penalty[22−25] $\sim \ln N$.

Since the CNT diameter *d* is constrained by the catalyst nanoparticle size,[26−28] typically it is assumed that the energy of the nanotube cap (comprising six pentagons) emerging from the initial nucleus is essentially independent of the CNT chirality. This simple argument allows one to focus

* Address correspondence to biy@rice.edu.

Received for review December 17, 2013 and accepted January 23, 2014.

Published online January 23, 2014
10.1021/nn406462e

exclusively on essential χ-dependent contributions to the total energy of the CNT−catalyst system, Figure 1, inset. Recently, Liu *et al.*[29] have analyzed the energetics of the CNT−catalyst interface based on atomistic calculations of the "edge" energy dependence on χ using graphene edge as a model. However, the attempts so far to quantify E^{cap} are scarce and limited to just a handful of caps and chiral indices (n,m),[30−32] although various aspects of the caps structure and energetics have been addressed in a number of studies.[13,17,33−40] The 1999 census of CNT caps,[41] however, has revealed rather crowded caps population where, empirically, the number of nanotube caps $N^{cap} \sim d^{\nu}$, with $\nu \simeq 8$.[30,41] This large exponent implies an enormous N^{cap} even for caps with isolated pentagons, leaving the effect of configurational diversity on CNT end-cap energetics practically unexplored, with the exception of perhaps a single study[30] of the (10, 0) zigzag tube with $N^{cap}_{10,0} = 7$.[41] Since any multiplicity of caps results in a configurational entropy contribution $S_{n,m} = k_B \ln N^{cap}_{n,m}$ (k_B = the Boltzmann constant, Figure 1), the strong diameter dependence of the cap numbers has been invoked early on to rationalize the experimentally observed preference for larger-diameter tubes.[42,43]

Such a configurational variety may informally be looked at from materials informatics perspective. A fixed pattern of six pentagons encodes what unique (n, m) chirality a nascent nanotube would inherit. In this sense it can be viewed as the "inorganic gene"[44,45] of a CNT. Although the chirality code is written in a single "letter" (a pentagon, unlike the four-letter DNA alphabet, for instance), its effective two-dimensionality (set by the sp^2 C hybridization) allows for multiple six-pentagon configurations that can be aptly "sequenced" in the language of graph theory.[41] The present effort thus aims to establish a quantitative structure−property (intrinsic elastic energy) relation for a set of more than 4500 caps representing 21 chiralities. This is achieved by a systematic study of CNT cap energetics over the *whole range* of chiral angles $0° \leqslant \chi \leqslant 30°$ based on large-scale atomistic calculations of *all* possible caps with isolated pentagons for selected values of d.

RESULTS AND DISCUSSION

Here we consider two sets of nanotubes, whose chiral angles sweep the full zigzag-to-armchair range, and correspond to two diameter constraints: $d \simeq 0.8$ nm ($N^{cap} = 89$) and $d \simeq 1$ nm ($N^{cap} = 4459$), respectively. Figure 1 shows N^{cap} for the selected (n,m) pairs. More details are given in the Methods section. Note that as χ varies, a d = const condition cannot be strictly fulfilled, and diameters differ by ~5%. In choosing the set of chiral indices, we have mandated that there exist at least two caps that would fit a given (n,m) tube, $N^{cap}_{n,m} > 1$, leading to smaller $d \simeq 0.8$ nm. The set representing $d \simeq 1$ nm has much larger N^{cap}, yet

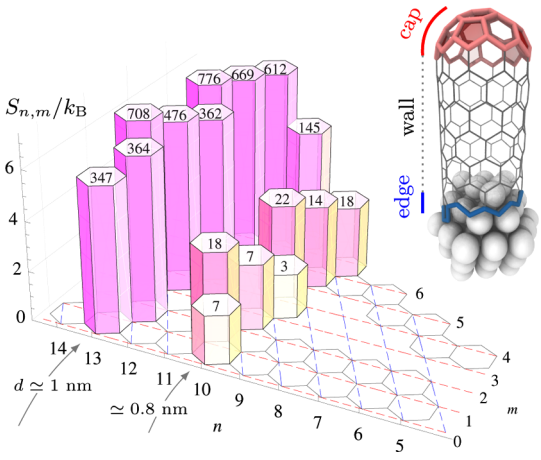

Figure 1. Configurational entropy $S_{n,m}$ associated with multiple possible nanotube end-caps with isolated pentagons for the (n,m) pairs considered in the present work. Actual cap numbers $N^{cap}_{n,m}$ are shown atop the corresponding prismatic bars (these figures are to be doubled for chiral tubes to account for left- and right-handed enantiomers). Inset: Schematic representation of (energy) partitioning for a CNT formed on a catalytic nanoparticle, with the CNT cap and edge highlighted.

feasible computationally. It is also the minimal diameter beyond which the number of caps appears to approach the $\sim d^8$ asymptotic dependence.[30]

Here we explore the ground-state energy landscape in terms of the CNT cap energy defined as

$$\begin{aligned} \varepsilon_{n,m} &= \varepsilon'_{n,m} - \mu_g \\ &\equiv \frac{1}{n_\cap}\left[E^{tot}_{n,m}(N) - (N - n_\cap)\mu^{CNT}_{n,m}\right] - \mu_g \end{aligned} \tag{1}$$

where $E^{tot}_{n,m}(N)$ is the total potential energy of the system of N carbon atoms representing the capped CNT for given (n,m), $\mu^{CNT}_{n,m}$ is the cohesive energy per atom in an ideal infinite CNT of the same chirality, μ_g is that for graphene, and $n_\cap$ is the number of atoms in the cap. As defined in eq 1, the cap energy is a *per atom* excess quantity, with graphene as a reference. The actual value of $n_\cap$ is linked to the particular cap enumeration algorithm and thereby subject to the provisions made in the literature[41,46] regarding the choice of a boundary between the CNT and the cap. An immediate implication is that such a boundary, as pointed out by Brinkmann *et al.*,[41,46] *e.g.*, for a capped (n,n) tube, may not be strictly of armchair type (see Figure 4 below). By construction, however, for given (n,m) the algorithm guarantees that the caps have identical embedding ($N-n_\cap$), or "layers" of hexagons, as described in the Methods section.

One can further rewrite eq 1 in an equivalent form

$$\varepsilon_{n,m} = \frac{1}{n_\cap}\Omega_{n,m} + \mu^{CNT}_{n,m} - \mu_g \tag{2}$$

to separate the CNT elastic bending energy[22,47−51] $\mu_{n,m}{}^{CNT} - \mu_g \sim 1/d^2$ inherent to the definition eq 1. The grand-potential term

$$\Omega_{n,m} \equiv E^{tot}_{n,m}(N) - N\mu^{CNT}_{n,m} \tag{3}$$

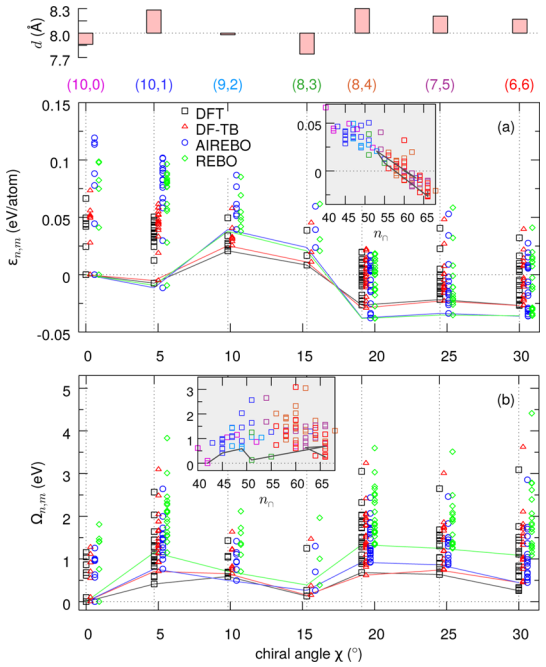

Figure 2. (a) Cap energy $\varepsilon_{n,m}$, according to eq 1, for all 89 caps with $d \simeq 0.8$ nm, relative to $\varepsilon_{10,0} \equiv \varepsilon_{\chi=0}$. Lines connect the minimal energies, $\min_i \varepsilon^{(i)}_{\chi=\text{const}}$, for given computational method. For clarity, calculated points are slightly offset for each method. The actual CNT diameters d are given in the top panel (bars, relative to a reference value $d_0 = 0.8$ nm). (b) Similar to (a), but for $\Omega_{n,m}$, according to eq 3. The insets show only the corresponding DFT-calculated quantities *vs* the number of C atoms in the cap $n_\cap$. Color coding is identical to that used for the (*n*,*m*) tick labels in (a).

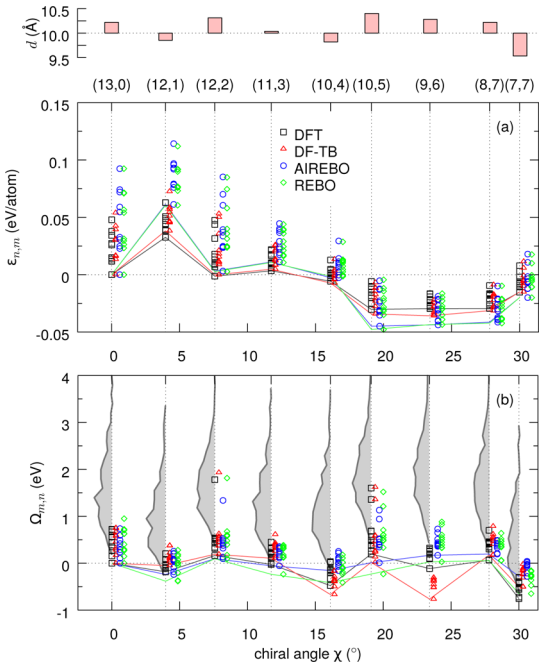

Figure 3. Similar to Figure 2, but for the set of caps with $d \simeq 1$ nm, relative to $\varepsilon_{13,0} \equiv \varepsilon_{\chi=0}$. The gray filled lines in (b) represent the energy histograms of *all* 4459 caps, calculated with DF-TB, using 0.2 eV bins.

is then the *total* energy cost of transforming a (*n*,*m*) CNT into a capped tube with the same number of atoms *N* and chirality and is invariant with respect to the cap−CNT boundary choice. Such definitions are indeed expedient in the context of the poorly defined boundary between the cap and the CNT, as already mentioned above. Without the $\mu^{\text{CNT}}_{n,m}$ term, "moving" the cap−CNT boundary, $n_\cap \rightarrow n_\cap \pm \Delta n_\cap$ (for example, excluding/adding a carbon dimer from/to a local armchair section of the initial boundary), would result in a bias $\Delta n_\cap(\mu^{\text{CNT}}_{n,m} - \mu_g)$.

All cap energies calculated from eq 1 for $d \simeq 0.8$ nm using two reactive bond-order empirical potentials (REBO and AIREBO) and two quantum-mechanical methods, density-functional theory (DFT) and DFT-based tight binding (DF-TB) (see the Methods section for computational details), are plotted in Figure 2a. The minimal $\varepsilon_{n,m}$, regardless of the computational method, lie in an energy window of ≃1 eV/atom, which for typical growth conditions is $\sim k_B T$, *T* being the temperature, with caps toward the armchair end displaying slightly lower $\varepsilon_{n,m}$ values. It is evident that the configurational minimization

$$\min_i \varepsilon^{(i)}_{\chi=\text{const}}, \quad 1 \leqslant i \leqslant N^{\text{cap}}_{n,m} \tag{4}$$

(*i* being the cap index for given (*n*,*m*), see also Figure 1), is crucial in assessing the relative stability, as the actual pentagonal pattern can bring about energy variation of up to ≃0.1 eV, especially when evaluation employs the empirical potentials.

The graph reveals clearly the scale of variation in the cap energies over the whole range of chiral angles. The configurationally minimal energies $\min_i \varepsilon^{(i)}_{n,m}$, Figure 2a, are those corresponding to the caps with largest $n_\cap$ for given (*n*,*m*); note that for some chiralities there exist a whole subset of $N^{\text{cap}}_{n,m}$ of caps (*i.e.*, more than one) with largest $n_\cap$. Ranking of higher-energy structures is however not monotonous with respect to $n_\cap$. The $\min\varepsilon_{n,m}$ variation with the chiral angle χ is very similar for all computational schemes employed; the DFT-based methods and the empirical potentials form two pairs, practically indistinguishable within the computational accuracy. It should be noted that DFT and DF-TB fully agree in identifying the same end-caps as lowest-energy configurations for practically all (*n*,*m*). Similarities between the methods are apparent also in the $\Omega_{n,m}$ plots, Figure 2b. As total quantities, $\Omega_{n,m}$ for given chirality vary over a wider energy scale, ∼1−3 eV, and qualitatively follow the trend in the CNT diameters *d*, whose actual values are given in the top panel of Figure 2. However, there is no clear correlation between the minimal-$\Omega_{n,m}$ envelope of all configuration and the size of the caps $n_\cap$, Figure 2b, inset.

The energetics of the larger CNT caps for $d \simeq 1.0$ nm requires computation of $E^{\text{tot}}_{n,m}$ of a huge number of structures, Figure 1, which is a daunting task especially at the DFT level. Exploiting the very good agreement between DFT and DF-TB for the smaller set, Figure 2,

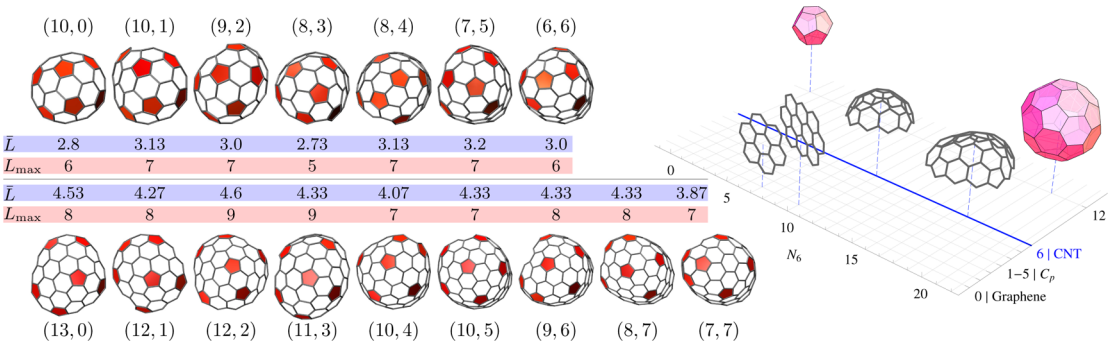

Figure 4. Cap geometries with the lowest $\Omega_{n,m}$ values calculated with DFT. All pentagonal rings are highlighted.[52,53] The largest element L_{max} and the mean of all elements $\bar{L}$ of the corresponding distance matrices, eq 5, are given as well. Inset: Schematic map of some cyclic carbon structures in the (N_6,N_5)-plane. The C_p lines correspond to cone structures[25] with p pentagons. All caps/CNT considered can be mapped onto the $N_5 = 6$ highlighted line. A few examples are explicitly rendered: the C_{20} dodecahedron at (0, 12), the C_{60} buckyball at (20, 12), the (10, 0)-cap at (11, 6) and (13, 0)-cap at (18, 6), coronine at (7, 0) and ovalene at (10, 0).

selection of structures to be calculated and compared for all the four methods was based on the DF-TB-calculated energies of all $N^{cap} = 4459$ configurations as explained in the Methods section. The energies of the reduced set of 90 structures for $d \simeq 1.0$ nm, calculated from eq 1 and eq 3, are plotted in Figure 3. We shall note that practically the whole discussion above regarding the energetics in Figure 2 is applicable also to the case of larger-diameter capped tubes, Figure 3. A representative example of all energies calculated with the DF-TB method is given in Figure 3b; because of the large number of structures we show the energy histograms that can be viewed as "density of cap states". Note that the configurational diversity accounts for ≃4 eV spread in $\Omega_{n,m}$. The lowest-$\Omega_{n,m}$ geometries of all 16 chiralities from Figure 2 and Figure 3 as obtained from DFT are rendered in Figure 4. As all caps incorporate exactly $N_5 = 6$ pentagons, there is one-to-one correspondence between $n_\cap$ and the number of hexagons N_6 in the cap. Thus, in the (N_5,N_6) plane, these structures are mapped onto a set of discrete points lying along the $N_5 = 6$ line as sketched in the inset of Figure 4.

It is well understood that among the possible configurations of six pentagons, those that obey the isolated-pentagon rule (as all geometries considered here do) are most favorable energetically.[30,54] Rationalizing the energy ranking within the sets of $N^{cap}_{n,m}$ structures for each (n,m) is no longer straightforward as alluded to in the studies on the isolated-pentagon fullerenes.[54] We have explored possible correlations between $\Omega_{n,m}$ and some basic characteristics of the corresponding cap graphs.[41,54] Specifically, we consider the pentagon−pentagon distance matrix L with elements

$$L_{pq} = (1 - \delta_{pq})l_{pq} \quad (5)$$

where δ_{pq} is the Kronecker delta and l_{pq} is the shortest path in terms of number of bonds that connects an atom from pentagon p with an atom from pentagon q. Note that the isolated-pentagon rule is simply equivalent to $\min_{p,q} L_{pq} \geqslant 1$. In Figure 4 we report the largest element (longest distance) L_{max} and the mean of all matrix elements $\bar{L}$ for the corresponding lowest-$\Omega_{n,m}$ geometries. We do not find, however, any systematic correlation between the energy ranking and the distance-based invariants of the cap graphs,[54] *e.g.*, hexagon neighbor index or those related to the spectrum of L.

The merit of quantifying the CNT cap energetics is best revealed when considering $\Omega_{n,m}$ in the two-dimensional parameter space (d, χ). It is straightforward to further extend the set of structures, Figure 1, with five trivial cases of (n,m) tubes, each having just a single isolated-pentagon cap: the achiral (9, 0) and (5, 5) with $d \simeq 0.7$ nm, and the chiral (9, 1), (8, 2), and (6, 5) tubes. The resulting extended set of points, calculated using DFT, is shown in Figure 5. In a zero-order approximation, the excess energy attributed to the CNT cap is considered as an essentially elastic curvature energy and thereby χ-independent,

$$\Omega_{n,m} \sim \ln d \quad (6)$$

Indeed, approximating the cap as a superposition of six "cones", one can write its elastic energy E in the form[22,24,25]

$$E = E_{core} + \frac{11}{5}\pi D \ln(\overline{r_{max}}/a) \quad (7)$$

where E_{core} is the local contribution from the pentagon disclinations, D the bending rigidity of graphene, $\overline{r_{max}} = (\Pi_p^6 r_{max,p})^{1/6}$ the geometric mean of the "lengths" of the six cones, and a is a cutoff of the order of the bond length. For the pth pentagon, $r_{max,p}$ may be chosen as half of the nearest-pentagon-neighbor distance, *i.e.*, $2r_{max,p}/a \sim \min_q L_{pq}$. The ln d-fit to the calculated points is given on the (d, Ω)-face of the plot in Figure 5 and results in $D \simeq 1.3$ eV in excellent agreement with the values $D \simeq 1.1-1.5$ eV reported in previous works using the same computational methods.[25,51,55] Within such a picture, the variation in the minimal cap energies from Figure 2b and Figure 3b appears to reflect the differences in the discrete

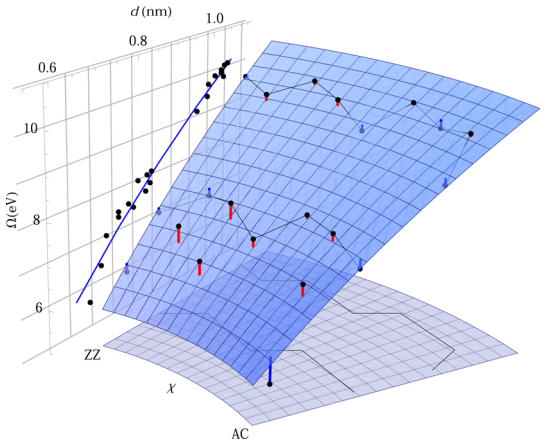

Figure 5. Polar plot of the $\Omega_{n,m}$ surface obtained by revolving the $\Omega_{n,m}(d)$ fit (blue curve on the (d, Ω)-face of the graph) to the calculated DFT points over the chiral angle $0° \leqslant \chi \leqslant 30°$. The two DFT data sets from Figure 2 and Figure 3 are extended with five trivial cases for which $N^{cap}_{n,m} \equiv 1$: (9, 0), (9, 1), (8, 2), (6, 5), and (5, 5). The distance of the calculated points to the analytical surface is indicated by impulses (above: red; below: blue).

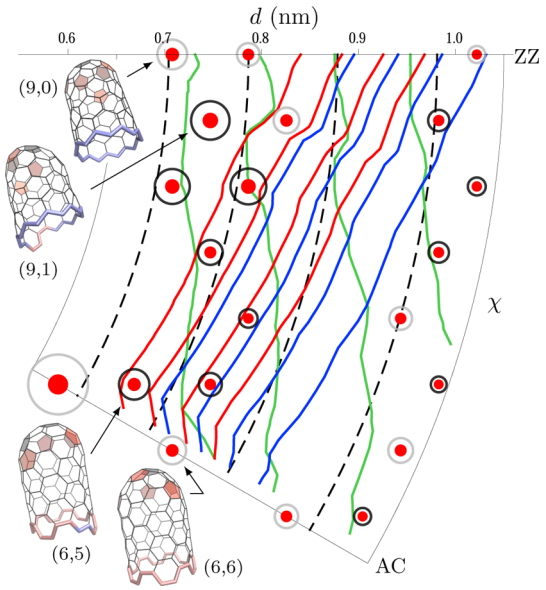

Figure 6. Polar plot of the $\Omega + \Gamma$ surface in the (d, χ) plane. The dashed contours correspond to the analytical Ω surface in Figure 5, and the open-circle sizes correspond to the impulse lengths in Figure 5. For clarity, only energy slices of 3 eV width are rendered, and isoenergy contour-line spacing is 1 eV in all cases. $\gamma_{AC,ZZ}$ edge energies, *cf.* eq 8, for hydrogen termination (green), using H_2 reservoir, are taken from ref 29 and for Fe (red) and Co (blue) from ref 56. Images illustrate a few geometries with both the pentagon pattern and edge highlighted.

tube diameter d (*cf.* the projected lines onto the base-plane of Figure 5). One can formally obtain a $\Omega(d, \chi)$ surface by revolving $\Omega(d)$ over the chiral angle $0° \leqslant \chi \leqslant 30°$, as shown in Figure 5.

The lack of intrinsic chiral preferences associated with the nanotube caps, as deduced from Figure 5, warrants the exploration of other routes toward χ-control. A possible, expedient approach might rest upon the theoretical scheme proposed in ref 29 that allowed us to quantify the energetics of graphene edge and, in particular, the sp^2-carbon−metal interface.[4,29,56] The chemical aspect to an interface-controlled scenario is that unlike the "chirally inert" capped end of a CNT, the open-edge (see inset in Figure 1) energy is χ-dependent,[29]

$$\begin{aligned}\gamma(\chi) &= 2\gamma_{AC}\sin\chi + 2\gamma_{ZZ}\sin(\pi/6 - \chi) \\ &= |\gamma|\cos(\chi + C),\end{aligned} \tag{8}$$

and can be fine-tuned ultimately through the chemical phase shift $C = C(\mu)$, μ being the chemical potential of the species in contact with the edge. Combining eq 8 with eq 3, one obtains the total excess energy of a capped CNT with a chemically modified open edge, $\Omega(d, \chi) + \Gamma(d, \chi)$, where $\Gamma(d, \chi) \equiv \pi d\gamma(\chi)$. The effect of different edge terminations is illustrated in Figure 6. The "distortion" of the reference (dashed) isoenergy contours, corresponding to the analytical surface in Figure 5, is a simple consequence of the term $\sim d \times \cos\chi$. In this case the $\Omega(d, \chi)$ surface is obtained by irregular-grid interpolation of the actual calculated points, which leads to a generally "rough" surface and thereby wiggled isoenergy contours. Note, however, that the dominant effect stems from the edge term, *viz.* the nature of the species in contact with the open CNT edge. Thus, within the thermodynamic arguments of ref 29, Co and Fe would render ZZ-edge preference, while hydrogen results in preferred AC edge.

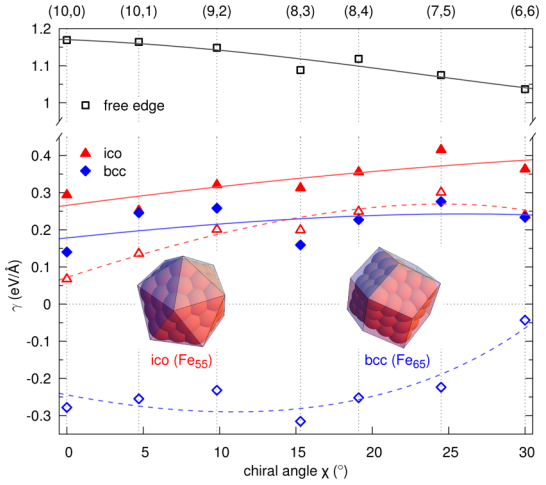

Figure 7. Comparison of the CNT/catalyst interface energies $\gamma(\chi)$ (symbols) of smaller-diameter tubes, *cf.* Figure 2, for a free edge and in contact with two Fe clusters of different shapes: an icosahedral Fe_{55} cluster (left image) and a rhombic dodecahedral bcc-Fe_{65} cluster (right image), as calculated with DF-TB. Open symbols correspond to values calculated without spin polarization. The lines are least-squares fits to the analytical expression, eq 8, also including a ZZ−AC mixing term.[29]

The dominant role of the CNT/catalyst interface can be illustrated by direct atomistic calculations of $\gamma(\chi)$ (see Methods section for details). For that purpose, we use the identified lowest-energy caps, corresponding to the set of chiralities from Figure 2, and arrange them for comparison on two Fe clusters of different shape: an

icosahedral Fe_{55} cluster and an Fe_{65} rhombic dodecahedron with a body-centered cubic (bcc) structure, Figure 7. $\gamma(\chi)$ of the individual free-edge tubes (essentially that of the pristine graphene edge[29]) is given as a reference, showing the familiar trend with preferred AC edge. On an Fe cluster this trend is reversed, as already seen in Figure 6. This example, using a *monoelemental* cluster, indicates that the catalyst shape and magnetic state may provide additional routes toward control of $\gamma(\chi)$. It is worth noting that for an assumed nonmagnetic state of the Fe_{65} cluster, the combined effect of the AC−ZZ mixing term and phase shift C leads to a convex $\gamma(\chi)$ and a negative interface energy,[29] with a local minimum closer to the center of the chirality range. For the magic-size icosahedral Fe_{55} cluster the magnetic state reflects merely in a constant shift for all but the ZZ interface.

CONCLUSIONS

Single-walled CNT are now routinely grown, and chirality distribution maps are abundant in the literature.[57−68] Chronologically, those experimental works seem to reveal a gradually emerging chiral selectivity, with some of the most recent experiments demonstrating unusually strong, and eventually puzzling, preference toward near-armchair CNTs.[67,68] Controlling the caps structure, and hence their energetics, has been deemed a possible route toward chiral selectivity in catalytic growth of CNTs. To provide rigorous quantitative basis for analysis, here we have presented a detailed mapping of the intrinsic elastic energy landscape of capped single-wall CNTs. The explicit account of multiple structural "isomers" (*i.e.*, the configurational variety of the six-pentagon pattern of the caps) essentially proves no viable correlation between the cap energetics and the chiral angle χ. Thus, the "end-caps" of a carbon nanotube do not display an intrinsic preference to a specific chirality (n,m), which leaves room for other approaches to control the chirality, especially by tuning the interaction between nanotube edge and catalyst[29] *via* the choice of material, catalyst shape, and possibly other state characteristics. The present work also provides valuable insights for the analysis of properties where the details in the pentagonal pattern of the CNT endcap are essential and have major imprint on its electronic structure.[69−72]

METHODS

Enumeration of all possible isolated-pentagon caps for given (n,m) and generation of the corresponding atomic coordinates were performed with the Chemical and Abstract Graph Environment CAGE.[73] The two-dimensional graphs output by CAGE were postprocessed by HyperChem software[74] to generate the initial three-dimensional Cartesian coordinates of the structures for subsequent optimization in other codes as explained below. The total number of caps generated was $N_{cap} = 4548$. Each final geometry represents the CNT cap along with three "layers" of hexagons from the nascent nanotube. Closed, fullerene *cages* were constructed from the single-cap (or "half-tube") geometries by duplication (therefore twice bigger number of atoms in the cage) followed by appropriate set of coordinate transformations.

Total energies were calculated within density-functional theory (DFT) using the SIESTA[75] code, the density-functional based tight-binding method (DF-TB) using the DFTB+ code,[76] and employing the AIREBO/REBO reactive bond-order empirical potentials[77,78] as implemented in the LAMMPS[79] simulator.

The DFT calculations were carried out using the PBE generalized gradient approximation functional[80] with a localized pseudoatomic orbital (double-ζ, polarized) basis set and Troullier−Martins norm-conserving pseudopotentials. The simulation cell was chosen so as to ensure at least 1 nm vacuum region between system images in a nonperiodic direction. For CNT calculations, Brillouin zone sampling along the axis was chosen so that the corresponding effective spatial cutoff was within the range of 8−11 nm for all tubes. Conjugate gradient scheme with force tolerance 0.01 eV/Å was used to optimize all geometries.

The self-consistent charge DF-TB calculations employ Slater−Koster parameters as provided in the pbc-0−3[81] and trans3d-0−1[82] sets. The CNT/catalyst interface energy in Figure 7 is defined as $\gamma = (E^{tot} - (1/2)E^{tot}_{n,m} - E_{Fe})/\pi d$, where E^{tot} is the energy of the CNT/Fe system, E_{Fe} is the energy of the free Fe cluster, and $E^{tot}_{n,m}$ is the energy of the closed CNT cage with minimal $\Omega_{n,m}$, for given (n,m), eq 3. The CNT axis in the initial geometry is along the 5-fold axis of the icosahedral Fe_{55} cluster, and along the 3-fold axis of the dodecahedral Fe_{65} cluster, respectively. Conjugate gradient optimization is performed with force tolerance of 0.05 eV/Å. Spin-polarized calculations are performed first for isolated cluster to determine the net magnetic moments. For the icosahedral Fe_{55} we reproduce the value 1.93 μ_B/atom (antiferromagnetic state) from the literature,[83] while the calculated magnetic moment for the bcc Fe_{65} cluster (ferromagnetic state) is 2.8 μ_B/atom. Geometry optimization of the CNT/Fe systems is performed keeping the magnetic moments on the Fe cluster collinear, setting the initial net values according to those determined for the isolated cluster.

The procedure for calculating the energetics of the larger caps for $d \simeq 1$ nm, due to their huge number, differs slightly from the one described above for the smaller-diameter tubes. All caps were optimized at all but the DFT level, using the as-generated[73] "half-tube" geometries. To subtract the energy contribution due to the open edge, an additional set of calculations has been carried out for long, *finite* CNTs with exactly the same edges as the caps. The edge structure of all half-tubes was parsed/verified with our EDGECOUNT tool.[84] As a second step, closed cages were generated only from the 10 half-tubes with lowest $\Omega_{n,m}$ for each chiral angle (only these $9 \times 10 = 90$ closed-cage structures were calculated with DFT).

To calculate various graph characteristics, we use the algorithm from ref 85 that implements the nilpotent adjacency matrix method for enumerating pentagonal and hexagonal cycles in the cap graphs.

Conflict of Interest: The authors declare no competing financial interest.

Acknowledgment. This work was supported by the Office of Naval Research Grant N00014-11-1077. Computer resources were provided by XSEDE, which is supported by NSF Grant OCI-1053575, under allocation TG-DMR100029 and the DAVinCI cluster acquired with funds from NSF grant OCI-0959097. E.P. would like to acknowledge discussions with Yuanyue Liu.

REFERENCES AND NOTES

1. Iijima, S. Helical Microtubules of Graphitic Carbon. *Nature* **1991**, *354*, 56–58.
2. Jin, C.; Suenaga, K.; Iijima, S. How Does a Carbon Nanotube Grow? An *In Situ* Investigation on the Cap Evolution. *ACS Nano* **2008**, *2*, 1275–1279.
3. Nesterenko, A. M.; Kolesnik, N. F.; Akhmatov, Y. S.; Suhomlin, V. I.; Prilutskii, O. V. Characteristics of the Phase Composition

and Structure of the Products of NiO and Fe_2O_3 Interaction With Carbon Monoxide. *Izv. Akad. Nauk SSSR, Met.* **1982**, *3*, 12–17, in Russian; UDK 669.173.23.
4. Penev, E. S.; Artyukhov, V. I.; Ding, F.; Yakobson, B. I. Unfolding the Fullerene: Nanotubes, Graphene and Poly-Elemental Varieties by Simulations. *Adv. Mater.* **2012**, *24*, 4956–4976.
5. Krishnan, A.; Dujardin, E.; Treacy, M. M. J.; Hugdahl, J.; Lynum, S.; Ebbesen, T. W. Graphitic Cones and the Nucleation of Curved Carbon Surfaces. *Nature* **1997**, *388*, 451–454.
6. Zhang, P.; Crespi, V. H. Nucleation of Carbon Nanotubes without Pentagonal Rings. *Phys. Rev. Lett.* **1999**, *83*, 1791–1794.
7. Kuznetsov, V. L.; Usoltseva, A. N.; Chuvilin, A. L.; Obraztsova, E. D.; Bonard, J. M. Thermodynamic Analysis of Nucleation of Carbon Deposits on Metal Particles and Its Implications for the Growth of Carbon Nanotubes. *Phys. Rev. B: Condens. Matter Mater. Phys.* **2001**, *64*, 235401.
8. Fan, X.; Buczko, R.; Puretzky, A. A.; Geohegan, D. B.; Howe, J. Y.; Pantelides, S. T.; Pennycook, S. J. Nucleation of Single-Walled Carbon Nanotubes. *Phys. Rev. Lett.* **2003**, *90*, 145501.
9. Wells, J. C.; Noid, D. W.; Sumpter, B. G.; Wood, R. F.; Zhang, Q. Multiscale Simulations of Carbon Nanotube Nucleation and Growth: Electronic Structure Calculations. *J. Nanosci. Nanotechnol.* **2004**, *4*, 414–422.
10. Amara, H.; Bichara, C.; Ducastelle, F. Understanding the Nucleation Mechanisms of Carbon Nanotubes in Catalytic Chemical Vapor Deposition. *Phys. Rev. Lett.* **2008**, *100*, 56105.
11. Moors, M.; Amara, H.; Visart de Bocarmé, T.; Bichara, C.; Ducastelle, F.; Kruse, N.; Charlier, J. C. Early Stages in the Nucleation Process of Carbon Nanotubes. *ACS Nano* **2009**, *3*, 511–516.
12. Ribas, M. A.; Ding, F.; Balbuena, P. B.; Yakobson, B. I. Nanotube Nucleation *versus* Carbon-Catalyst Adhesion-Probed by Molecular Dynamics Simulations. *J. Chem. Phys.* **2009**, *131*, 224501.
13. Ohta, Y.; Okamoto, Y.; Page, A. J.; Irle, S.; Morokuma, K. Quantum Chemical Molecular Dynamics Simulation of Single-Walled Carbon Nanotube Cap Nucleation on an Iron Particle. *ACS Nano* **2009**, *3*, 3413–3420.
14. Schebarchov, D.; Hendy, S. C.; Ertekin, E.; Grossman, J. C. Interplay of Wetting and Elasticity in the Nucleation of Carbon Nanotubes. *Phys. Rev. Lett.* **2011**, *107*, 185503.
15. Pigos, E.; Penev, E. S.; Ribas, M. A.; Sharma, R.; Yakobson, B. I.; Harutyunyan, A. R. Carbon Nanotube Nucleation Driven by Catalyst Morphology Dynamics. *ACS Nano* **2011**, *5*, 10096–10101.
16. Lacovig, P.; Pozzo, M.; Alfe, D.; Vilmercati, P.; Baraldi, A.; Lizzit, S. Growth of Dome-Shaped Carbon Nanoislands on Ir (111): the Intermediate between Carbidic Clusters and Quasi-Free-Standing Graphene. *Phys. Rev. Lett.* **2009**, *103*, 166101.
17. Wang, B.; Ma, X.; Caffio, M.; Schaub, R.; Li, W.-X. Size-Selective Carbon Nanoclusters as Precursors to the Growth of Epitaxial Graphene. *Nano Lett.* **2011**, *11*, 424–430.
18. Yuan, Q.; Gao, J.; Shu, H.; Zhao, J.; Chen, X.; Ding, F. Magic Carbon Clusters in the Chemical Vapor Deposition Growth of Graphene. *J. Am. Chem. Soc.* **2012**, *134*, 2970–2975.
19. Gao, J.; Yip, J.; Zhao, J.; Yakobson, B. I.; Ding, F. Graphene Nucleation on Transition Metal Surface: Structure Transformation and Role of the Metal Step Edge. *J. Am. Chem. Soc.* **2011**, *133*, 5009–5015.
20. Lin, Y.; Ding, F.; Yakobson, B. Hydrogen Storage by Spillover on Graphene as a Phase Nucleation Process. *Phys. Rev. B: Condens. Matter Mater. Phys.* **2008**, *78*, 041402.
21. Singh, A. K.; Penev, E. S.; Yakobson, B. I. Vacancy Clusters in Graphane as Quantum Dots. *ACS Nano* **2010**, *4*, 3510–3514.
22. Tersoff, J. Energies of Fullerenes. *Phys. Rev. B: Condens. Matter Mater. Phys.* **1992**, *46*, 15546.
23. Kanzow, H.; Lenski, C.; Ding, A. Single-Wall Carbon Nanotube Diameter Distributions Calculated from Experimental Parameters. *Phys. Rev. B: Condens. Matter Mater. Phys.* **2001**, *63*, 125402.
24. Šiber, A. Energies of sp^2 Carbon Shapes with Pentagonal Disclinations and Elasticity Theory. *Nanotechnology* **2006**, *17*, 3598.
25. Liu, Y.; Yakobson, B. I. Cones, Pringles, and Grain Boundary Landscapes in Graphene Topology. *Nano Lett.* **2010**, *10*, 2178–2183.
26. Zhang, Y.; Li, Y.; Kim, W.; Wang, D.; Dai, H. Imaging As-Grown Single-Walled Carbon Nanotubes Originated from Isolated Catalytic Nanoparticles. *Appl. Phys. A: Mater. Sci. Process.* **2002**, *74*, 325–328.
27. Nasibulin, A. G.; Pikhitsa, P. V.; Jiang, H.; Kauppinen, E. I. Correlation between Catalyst Particle and Single-Walled Carbon Nanotube Diameters. *Carbon* **2005**, *43*, 2251–2257.
28. Fiawoo, M.-F. C.; Bonnot, A.-M.; Amara, H.; Bichara, C.; Thibault-Pénisson, J.; Loiseau, A. Evidence of Correlation between Catalyst Particles and the Single-Wall Carbon Nanotube Diameter: A First Step towards Chirality Control. *Phys. Rev. Lett.* **2012**, *108*, 195503.
29. Liu, Y.; Dobrinsky, A.; Yakobson, B. I. Graphene Edge from Armchair to Zigzag: The Origins of Nanotube Chirality? *Phys. Rev. Lett.* **2010**, *105*, 235502.
30. Reich, S.; Li, L.; Robertson, J. Structure and Formation Energy of Carbon Nanotube Caps. *Phys. Rev. B: Condens. Matter Mater. Phys.* **2005**, *72*, 165423.
31. Reich, S.; Li, L.; Robertson, J. Control the Chirality of Carbon Nanotubes by Epitaxial Growth. *Chem. Phys. Lett.* **2006**, *421*, 469–472.
32. Reich, S.; Li, L.; Robertson, J. Epitaxial Growth of Carbon Caps on Ni for Chiral Selectivity. *Phys. Status Solidi B* **2006**, *243*, 3494–3499.
33. Lair, S. L.; Herndon, W. C.; Murr, L. E.; Quinones, S. A. End Cap Nucleation of Carbon Nanotubes. *Carbon* **2006**, *44*, 447–455.
34. Gómez-Gualdrón, D. A.; Balbuena, P. B. The Role of Cap Chirality in the Mechanism of Growth of Single-Wall Carbon Nanotubes. *Nanotechnology* **2008**, *19*, 485604.
35. Gómez-Gualdrón, D. A.; McKenzie, G. D.; Alvarado, J. F. J.; Balbuena, P. B. Dynamic Evolution of Supported Metal Nanocatalyst/Carbon Structure during Single-Walled Carbon Nanotube Growth. *ACS Nano* **2012**, *6*, 720–735.
36. Zhao, J.; Balbuena, P. B. Effect of Nanotube Cap on the Aromaticity of Single-Wall Carbon Nanotubes. *J. Phys. Chem. C* **2008**, *112*, 13175–13180.
37. Wang, Q.; Ng, M. F.; Yang, S. W.; Yang, Y.; Chen, Y. The Mechanism of Single-Walled Carbon Nanotube Growth and Chirality Selection Induced by Carbon Atom and Dimer Addition. *ACS Nano* **2010**, *4*, 939–946.
38. Zhu, W.; Börjesson, A.; Bolton, K. DFT and Tight Binding Monte Carlo Calculations Related to Single-Walled Carbon Nanotube Nucleation and Growth. *Carbon* **2010**, *48*, 470–478.
39. Wang, Q.; Wang, H.; Wei, L.; Yang, S.-W.; Chen, Y. Reactive Sites for Chiral Selective Growth of Single-Walled Carbon Nanotubes: A DFT Study of Ni_{55}—C_n Complexes. *J. Phys. Chem. A* **2012**, *116*, 11709–11717.
40. Dutta, D.; Chiang, W.-H.; Sankaran, R. M.; Bhethanabotla, V. R. Epitaxial Nucleation Model for Chiral-Selective Growth of Single-Walled Carbon Nanotubes on Bimetallic Catalyst Surfaces. *Carbon* **2012**, *50*, 3766–3773.
41. Brinkmann, G.; Fowler, P. W.; Manolopoulos, D. E.; Palser, A. H. R. A Census of Nanotube Caps. *Chem. Phys. Lett.* **1999**, *315*, 335–347.
42. Dresselhaus, M. S.; Dresselhaus, G.; Saito, R. Physics of Carbon Nanotubes. *Carbon* **1995**, *33*, 883–891.
43. Dresselhaus, M. S.; Dresselhaus, G.; Eklund, P. C. *Science of Fullerenes and Carbon Nanotubes*; Academic Press: San Diego, CA, 1996; Chapter 19.
44. Mackay, A. L. From "The Dialectics of Nature" to the Inorganic Gene. *Found. Chem.* **1999**, *1*, 43–56.
45. Delgado Friedrichs, O.; Dress, A. W. M.; Huson, D. H.; Klinowski, J.; Mackay, A. L. Systematic Enumeration of Crystalline Networks. *Nature* **1999**, *400*, 644–647.
46. Brinkmann, G.; Nathusius, U. v.; Palser, A. H. R. A Constructive Enumeration of Nanotube Caps. *Discrete Appl. Math.* **2002**, *116*, 55–71.

47. Adams, G. B.; Sankey, O. F.; Page, J. B.; O'Keeffe, M.; Drabold, D. Energetics of Large Fullerenes: Balls, Tubes, and Capsules. *Science* **1992**, *256*, 1792–1795.
48. Robertson, D. H.; Brenner, D. W.; Mintmire, J. W. Energetics of Nanoscale Graphitic Tubules. *Phys. Rev. B: Condens. Matter Mater. Phys.* **1992**, *45*, 12592–12595.
49. Sawada, S.; Hamada, N. Energetics of Carbon Nano-Tubes. *Solid State Commun.* **1992**, *83*, 917–919.
50. Tománek, D.; Zhong, W.; Krastev, E. Stability of Multishell Fullerenes. *Phys. Rev. B: Condens. Matter Mater. Phys.* **1993**, *48*, 15461–15464.
51. Muñoz, E.; Singh, A. K.; Ribas, M. A.; Penev, E. S.; Yakobson, B. I. The Ultimate Diamond Slab: GraphAne *versus* GraphEne. *Diamond Relat. Mater.* **2010**, *19*, 368–373.
52. Humphrey, W.; Dalke, A.; Schulten, K. VMD – Visual Molecular Dynamics. *J. Mol. Graphics* **1996**, *14*, 33–38.
53. Cross, S.; Kuttel, M. M.; Stone, J. E.; Gain, J. E. Visualisation of Cyclic and Multi-Branched Molecules with VMD. *J. Mol. Graphics Modell.* **2009**, *28*, 131–139.
54. Fowler, P. W.; Caporossi, G.; Hansen, P. Distance Matrices, Wiener Indices, and Related Invariants of Fullerenes. *J. Phys. Chem. A* **2001**, *105*, 6232–6242.
55. Kudin, K. N.; Scuseria, G. E.; Yakobson, B. I. C_2F, BN, and C Nanoshell Elasticity from *Ab Initio* Computations. *Phys. Rev. B: Condens. Matter Mater. Phys.* **2001**, *64*, 235406.
56. Artyukhov, V. I.; Liu, Y.; Yakobson, B. I. Equilibrium at the Edge and Atomistic Mechanisms of Graphene Growth. *Proc. Natl. Acad. Sci. U. S. A.* **2012**, *109*, 15136–15140.
57. Jorio, A.; Saito, R.; Hafner, J. H.; Lieber, C. M.; Hunter, M.; McClure, T.; Dresselhaus, G.; Dresselhaus, M. S. Structural (*n*,*m*) Determination of Isolated Single-Wall Carbon Nanotubes by Resonant Raman Scattering. *Phys. Rev. Lett.* **2001**, *86*, 1118–1121.
58. Bachilo, S. M.; Balzano, L.; Herrera, J. E.; Pompeo, F.; Resasco, D. E.; Weisman, R. B. Narrow (*n*,*m*)-Distribution of Single-Walled Carbon Nanotubes Grown Using a Solid Supported Catalyst. *J. Am. Chem. Soc.* **2003**, *125*, 11186–11187.
59. Sato, Y.; Yanagi, K.; Miyata, Y.; Suenaga, K.; Kataura, H.; Iijima, S. Chiral-Angle Distribution for Separated Single-Walled Carbon Nanotubes. *Nano Lett.* **2008**, *8*, 3151–3154.
60. Chiang, W.-H.; Sankaran, R. M. Linking Catalyst Composition to Chirality Distributions of As-Grown Single-Walled Carbon Nanotubes by Tuning Ni_xFe_{1-x} Nanoparticles. *Nat. Mater.* **2009**, *8*, 882–886.
61. Chiang, W.-H.; Sakr, M.; Gao, X. P. A.; Sankaran, R. M. Nanoengineering Ni_xFe_{1-x} Catalysts for Gas-Phase, Selective Synthesis of Semiconducting Single-Walled Carbon Nanotubes. *ACS Nano* **2009**, *3*, 4023–4032.
62. Fouquet, M.; Hofmann, S.; Thomsen, C.; Robertson, J. Analysis of Carbon Nanotube Chiralities Obtained from a Bimetallic Co-Mo Catalyst. *Phys. Status Solidi B* **2010**, *247*, 2660–2663.
63. Wijeratne, S. S.; Harris, N. C.; Kiang, C.-H. Helicity Distributions of Single-Walled Carbon Nanotubes and Its Implication on the Growth Mechanism. *Materials* **2010**, *3*, 2725–2734.
64. Kato, T.; Hatakeyama, R. Direct Growth of Short Single-Walled Carbon Nanotubes with Narrow-Chirality Distribution by Time-Programmed Plasma Chemical Vapor Deposition. *ACS Nano* **2010**, *4*, 7395–7400.
65. Zhu, Z.; Jiang, H.; Susi, T.; Nasibulin, A. G.; Kauppinen, E. I. The Use of NH_3 to Promote the Production of Large-Diameter Single-Walled Carbon Nanotubes with a Narrow (*n*,*m*) Distribution. *J. Am. Chem. Soc.* **2011**, *133*, 1224–1227.
66. Fouquet, M.; Bayer, B. C.; Esconjauregui, S.; Blume, R.; Warner, J. H.; Hofmann, S.; Schlögl, R.; Thomsen, C.; Robertson, J. Highly Chiral-Selective Growth of Single-Walled Carbon Nanotubes with a Simple Monometallic Co Catalyst. *Phys. Rev. B: Condens. Matter Mater. Phys.* **2012**, *85*, 235411.
67. He, M.; Jiang, H.; Liu, B.; Fedotov, P. V.; Chernov, A. I.; Obraztsova, E. D.; Cavalca, F.; Wagner, J. B.; Hansen, T. W.; Anoshkin, I. V.; *et al.* Chiral-Selective Growth of Single-Walled Carbon Nanotubes on Lattice-Mismatched Epitaxial Cobalt Nanoparticles. *Sci. Rep.* **2013**, *3*, 1460.
68. Wang, H.; Wei, L.; Ren, F.; Wang, Q.; Pfefferle, L. D.; Haller, G. L.; Chen, Y. Chiral-Selective $CoSO_4/SiO_2$ Catalyst for (9, 8) Single-Walled Carbon Nanotube Growth. *ACS Nano* **2013**, *7*, 614–626.
69. Carroll, D. L.; Redlich, P.; Ajayan, P. M.; Charlier, J. C.; Blase, X.; De Vita, A.; Car, R. Electronic Structure and Localized States at Carbon Nanotube Tips. *Phys. Rev. Lett.* **1997**, *78*, 2811–2814.
70. Khazaei, S.; Khazaei, M.; Cheraghchi, H.; Daadmehr, V.; Kawazoe, Y. Considering the Effect of Different Arrangements of Pentagons on Density of States of Capped Carbon Nanotubes. *Physica B* **2011**, *406*, 3885–3890.
71. Khazaei, M.; Dean, K. A.; Farajian, A. A.; Kawazoe, Y. Field Emission Signature of Pentagons at Carbon Nanotube Caps. *J. Phys. Chem. C* **2007**, *111*, 6690–6693.
72. Marchand, M.; Journet, C.; Guillot, D.; Benoit, J.-M.; Yakobson, B. I.; Purcell, S. T. Growing a Carbon Nanotube Atom by Atom: "And Yet It Does Turn". *Nano Lett.* **2009**, *9*, 2961–2966.
73. Brinkmann, G.; Delgado Friedrichs, O.; Lisken, S.; Peeters, A.; Van Cleemput, N. CaGe—A Virtual Environment for Studying Some Special Classes of Plane Graphs—An Update. *MATCH Commun. Math. Comput. Chem.* **2010**, *63*, 533–552.
74. *HyperChem(TM) Professional*, 7.51; Hypercube, Inc.: Gainesville, FL.
75. Soler, J. M.; Artacho, E.; Gale, J.; García, A.; Junquera, J.; Ordejón, P.; Sánchez-Portal, D. The SIESTA Method for *Ab Initio* Order-N Materials Simulation. *J. Phys.: Condens. Matter* **2002**, *14*, 2745–2779.
76. Aradi, B.; Hourahine, B.; Frauenheim, T. DFTB+, A Sparse Matrix-Based Implementation of the DFTB Method. *J. Phys. Chem. A* **2007**, *111*, 5678–5684.
77. Stuart, S. J.; Tutein, A. B.; Harrison, J. A. A Reactive Potential for Hydrocarbons with Intermolecular Interactions. *J. Chem. Phys.* **2000**, *112*, 6472–6486.
78. Brenner, D. W.; Shenderova, O. A.; Harrison, J. A.; Stuart, S. J.; Ni, B.; Sinnott, S. B. A Second-Generation Reactive Empirical Bond Order (REBO) Potential Energy Expression for Hydrocarbons. *J. Phys.: Condens. Matter* **2002**, *14*, 783–802.
79. Plimpton, S. J. Fast Parallel Algorithms for Short-Range Molecular Dynamics. *J. Comput. Phys.* **1995**, *117*, 1–19.
80. Perdew, J. P.; Burke, K.; Ernzerhof, M. Generalized Gradient Approximation Made Simple. *Phys. Rev. Lett.* **1996**, *77*, 3865–3868.
81. Porezag, D.; Frauenheim, T.; Köhler, T.; Seifert, G.; Kaschner, R. Construction of Tight-Binding-Like Potentials on the Basis of Density-Functional Theory: Application to Carbon. *Phys. Rev. B: Condens. Matter Mater. Phys.* **1995**, *51*, 12947–12957.
82. Zheng, G.; Witek, H. A.; Bobadova-Parvanova, P.; Irle, S.; Musaev, D. G.; Prabhakar, R.; Morokuma, K.; Lundberg, M.; Elstner, M.; Köhler, C.; *et al.* Parameter Calibration of Transition-Metal Elements for the Spin-Polarized Self-Consistent-Charge Density-Functional Tight-Binding (DFTB) Method: Sc, Ti, Fe, Co, and Ni. *J. Chem. Theory Comput.* **2007**, *3*, 1349–1367.
83. Köhler, C.; Seifert, G.; Frauenheim, T. Magnetism and the Potential Energy Hypersurfaces of Fe_{53} to Fe_{57}. *Comput. Mater. Sci.* **2006**, *35*, 297–301.
84. Singh, A. K.; Penev, E. S.; Yakobson, B. I. Armchair or Zigzag? A Tool for Characterizing Graphene Edge. *Comput. Phys. Commun.* **2011**, *182*, 804–807.
85. Schott, R.; Stacey Staples, G. In *Guide to Geometric Algebra in Practice*; Dorst, L., Lasenby, J., Eds.; Springer: New York, 2011; pp 233–249.